

The DNA Nucleobase Thymine in Motion – Intersystem Crossing Simulated with Surface Hopping [☆]

Sebastian Mai^a, Martin Richter^{a,1}, Philipp Marquetand^{a,*}, Leticia González^{a,*}

^a*Institute of Theoretical Chemistry, Faculty of Chemistry, University of Vienna, Währinger Str. 17, 1090 Vienna, Austria.*

Abstract

We report ab initio excited-state dynamics simulations on isolated thymine to investigate the mechanism of intersystem crossing, based on CASSCF potential energy surfaces and the SHARC surface hopping method. We show that even though $S_2 \rightarrow S_1$ internal conversion is not described accurately with CASSCF, intersystem crossing can be correctly simulated. Intersystem crossing in thymine occurs from the S_1 ($^1n\pi^*$) minimum, via a nearby crossing with T_2 ($^3\pi\pi^*$). The system further relaxes via ultrafast internal conversion in the triplet manifold to the T_1 ($^3\pi\pi^*$) state. The simulations reveal that, once the system is trapped in the $^1n\pi^*$ minimum, intersystem crossing might proceed with a time constant of 1 ps. Furthermore, the change of the system's electronic state is accompanied respectively by elongation/shortening of specific bonds, which could thus be used as indicators to identify which state is populated in the dynamics.

Keywords: photochemistry, nonadiabatic dynamics, intersystem crossing, DNA, thymine

1. Introduction

DNA and RNA are among the primary absorbers of UV light in all known organisms, stemming from the large absorption cross-section of the nucleobases which are part of DNA and RNA strands. Absorption of UV light by the nucleobases leads to the formation of excited electronic states, which for this class of compounds mostly deactivate to the electronic ground state within a few ps [1–5]. A very small fraction of excitations of nucleobases in DNA leads to the formation of photochemical products called photolesions, which constitute damage to DNA/RNA and interferes with normal cellular processes. Among the photolesions, the dimerization of thymine to generate cyclobutane pyrimidine dimers is the most common one [6–9]. Because of this relevance, the photophysical and photochemical properties of thymine were studied intensively in the last decades.

Among the most controversial aspects of thymine's excited-state dynamics is the importance of intersystem crossing (ISC). ISC is the radiationless transition between states of different multiplicities, in particular from the initially populated singlet states to triplet states. Due to the high reactivity and long lifetime of triplet states, once formed, those states could be involved in the formation of photolesions like cyclobutane pyrimidine dimers and pyrimidine 6-4 pyrimidone adducts, as was suggested in the literature [10]. However, other authors have argued that these photolesions are formed without the involvement of triplet states [11, 12], or at least that triplet states only marginally contribute to these reactions [13, 14]. For these reasons, it is interesting to study the photophysics of thymine. Besides studies in biological environments, also photophysical investigations in solution and in the gas phase are important here, since they allow separating the intrinsic dynamics of thymine from the effect of the surrounding.

Measurements in aqueous solutions find that ISC yields are 0.004 [15] to 0.006 [16], while in chloroform the yield is 0.08 [17]. In acetonitrile the reported values range from 0.06 [16] to 0.18 [18], suggesting that ISC in thymine is solvent dependent.

[☆]This paper is dedicated to Professor Lorenz S. Cederbaum on the occasion of his 70th birthday.

*Corresponding author

Email addresses: philipp.marquetand@univie.ac.at (Philipp Marquetand), leticia.gonzalez@univie.ac.at (Leticia González)

¹Present address: Max-Born-Institute for Nonlinear Optics and Short Pulse Spectroscopy, 12489 Berlin, Germany.

dent and that less polar solvents enhance ISC. More recently, much effort has been devoted to use time-resolved experimental methods to probe the ultrafast dynamics of thymine. Gas phase pump-probe experiments are reported by several groups [19–26]; mostly a sub-ps and a few-ps (5–7 ps) time constant were found, some groups also reported a ns time constant [19, 22–25]. In aqueous solution, Hare et al. have shown that thymine decays biexponentially with two time constants of 2.8 and 30 ps [27].

Nevertheless, an assignment of the experimental time constants to either internal conversion or ISC is difficult solely based on the experimental data and hence the last years have seen a large number of theoretical calculations on thymine. A number of authors have optimized excited-state minima and crossing points, as well as calculated various paths between these geometries [28–37]. Some authors have also investigated possible stationary pathways for intersystem crossing [34, 38], showing that ISC is feasible through several singlet-triplet crossing points along its relaxation pathway. Furthermore, a number of non-adiabatic dynamics studies were performed [30, 32, 35, 39–42], but none included the possibility of ISC.

Thus, a logical next step in the investigation of intersystem crossing in thymine is to perform non-adiabatic dynamics simulations including singlet and triplet states with the possibility of ISC. The SHARC (Surface Hopping including ARbitrary Couplings) excited-state dynamics methodology [43–45] is especially well suited for this application, and has already been used successfully for describing ISC in other pyrimidine nucleobases [46–48].

2. Methodology

We performed non-adiabatic molecular dynamics simulations on thymine using the SHARC methodology [43–45]. The SHARC method is an extension of Tully’s fewest switches surface hopping [49], allowing to include in the simulations of all kinds of electronic couplings between the states, in particular spin-orbit couplings which enable ISC. The electronic Hamiltonian matrix involving the singlet and triplet states of interest (those states are eigenstates of the molecular Coulomb Hamiltonian, hence we denote these states as “MCH” states, see also Ref. [44]) including spin-orbit matrix elements is diagonalized to obtain spin-mixed, fully adiabatic states (called “diagonal states” in the following). The surface hopping procedure is then performed

on these diagonal states, with the gradients and surface hopping probabilities in the diagonal basis obtained as described in Ref. [44]. This methodology allows to treat internal conversion and ISC on the same footing, giving a balanced description of all non-radiative processes.

The dynamics simulations were based on SA(4+3)-CASSCF(12,9)/6-31G* (state-averaging over 4 singlets and 3 triplets, complete active space self-consistent field with an active space of 12 electrons in 9 orbitals) calculations performed with MOLPRO 2012 [50]. The active space contained 8 π/π^* orbitals and the lone pair of oxygen O_4 (ortho to the methyl group), while the lone pair of the other oxygen atom was excluded from the active space, since the $n\pi^*$ states involving excitation from this orbital are very high in energy.

The CASSCF method generally offers a good compromise between accuracy and performance, allowing to simulate an ensemble of sufficient size to sample the ISC channel of the thymine dynamics. However, it is known that CASSCF does not describe all aspects of the excited-state potential energy surfaces (PES) of thymine correctly [30, 32, 35, 37, 40]. In particular, CASSCF tends to significantly overestimate the energy of the $^1\pi\pi^*$ state (see Table S1 in the Supplementary Information (SI)), which not only affects the Franck-Condon region, but also the minimum [37] and the corresponding conical intersections; consequently, CASSCF will not be able to accurately describe the details of the $^1\pi\pi^*$ deactivation. Hence, here we will focus on the mechanism which brings about ISC. An investigation of this mechanism is possible with the CASSCF method, since the vicinity of the S_1 ($^1n\pi^*$) minimum and the crossings with the two lowest triplet states T_1 and T_2 are described properly on CASSCF level of theory, as compared to more accurate CASPT2 (Complete Active Space Perturbation Theory of 2nd order) [34], as will be shown below (see also the SI for a comparison of the two levels of theory).

Even though our primary focus is on the ISC mechanism of thymine, we simulated the full dynamics based on excitation to the bright states in the Franck-Condon region, in order to facilitate comparison with previous CASSCF dynamics studies on thymine [30, 32, 35, 42] and uracil [47, 51]. The initial conditions for the dynamics simulations were sampled from a Wigner distribution around the S_0 minimum geometry based on a frequency calculation at the SS-CASSCF(12,9)/6-31G* level of

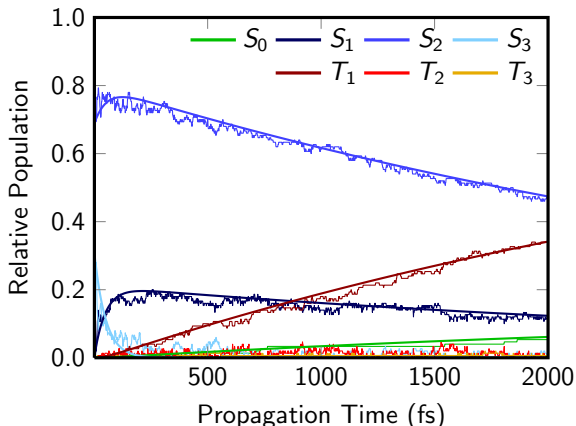


Figure 1: Population of MCH states of thymine averaged over 150 trajectories. The fitted populations based on the kinetic model described in the text are also shown.

theory. The initial excited state for each initial condition was determined stochastically, as proposed in Ref. [52]. Based on these initial conditions, an ensemble of 150 trajectories—107 trajectories starting from S_2 and 43 from S_3 —was propagated for up to 2 ps (less if a trajectory relaxed earlier to S_0 or T_1) with a timestep of 0.25 fs. Gradients and non-adiabatic coupling vectors were computed for states which are closer than 0.02 a.u. to the currently active state.

We note that even though the dynamics simulations were performed in the basis of the diagonal states (4 singlets and 3×3 triplets, giving 13 states in total), final analysis of the populations employed a transformation to the MCH states, which are easier to interpret, since they have defined multiplicities. Due to the large S_1 – S_2 energy gap, during the simulations the S_1 is $^1n\pi^*$ and S_2 is $^1\pi\pi^*$, so these labels can be used interchangeably. However, the two triplet states of $^3n\pi^*$ and $^3\pi\pi^*$ character often cross in the dynamics, so that there is no one-to-one correspondence to the states T_1 (energetically lower triplet state) and T_2 (upper triplet state).

3. Results and Discussion

Figure 1 shows the time-dependent populations of the MCH states averaged over the full ensemble as well as the curves resulting from a global fit, which will be described below. The figure shows that initially both the S_2 ($\pi\pi^*$) and S_3 ($\pi\pi^*$) are populated, but the S_3 ($\pi\pi^*$) is rapidly depopulated and does not play a significant role in the dynamics after about 200 fs. Population transfer from

S_2 ($\pi\pi^*$) to S_1 ($n\pi^*$) is much slower and consequently the S_2 ($\pi\pi^*$) population reaches about 80% after a few fs. Interestingly, the initial population transfer rate from S_2 ($\pi\pi^*$) to S_1 ($n\pi^*$) is quite large, and within 70 fs 20% of the total population reaches the S_1 . However, for later times the transfer rate becomes much smaller, and even after 2 ps almost 50% of the total population resides in the S_2 ($\pi\pi^*$). It appears that S_2 ($\pi\pi^*$) \rightarrow S_1 ($n\pi^*$) population transfer might occur via two channels, where the faster channel is quickly closed as the dynamics proceeds. From S_1 ($n\pi^*$), two relaxation pathways are available: relaxation to the S_0 and ISC to the triplet manifold with subsequent relaxation to T_1 . Based on the populations, ISC seems to be the more competitive pathway, since within 2 ps the T_1 population increases to about 35%, while the S_0 population only reaches 5% (8 trajectories). These findings are qualitatively similar to our previous results on uracil, which also shows the mentioned two-step decay of the S_2 ($\pi\pi^*$) and more ISC than relaxation to the ground state [47].

In order to obtain rate constants for the population transfer in thymine, a global fit procedure was performed. The global fit is based on the kinetic model shown in figure 2, including 6 species (S_3 , fast S_2 , slow S_2 , S_1 , S_0 and T_1) and six time constants ($S_3 \rightarrow S_2^{\text{fast}}$, $S_2^{\text{fast}} \rightarrow S_2^{\text{slow}}$, $S_2^{\text{fast}} \rightarrow S_1$, $S_2^{\text{slow}} \rightarrow S_1$, $S_1 \rightarrow S_0$ and $S_1 \rightarrow T_1$); see also the Supplementary Information for more details regarding the fitting procedure. Since the populations of T_2 and T_3 are always very small (on average, the sum of their populations is 2%), they were neglected in the global fit procedure (but note that the T_2 is very important for the ISC mechanism, just $T_2 \rightarrow T_1$ IC is extremely fast and hence T_2 does not acquire a sizeable population). A simpler model ($S_3 \rightarrow S_2 \rightarrow S_1 \rightarrow S_0$ and $S_1 \rightarrow T_1$) was also tested but fails to describe the fast initial rise of the S_1 population, so that the more complex model with two paths from S_2 to S_1 had to be employed. The fitted time constants are given in Figure 2, showing that $S_3 \rightarrow S_2$ has a time constant of 50 fs, $S_2 \rightarrow S_1$ has two time constants of 160 and 3800 fs, relaxation to S_0 has 5200 fs and ISC has 900 fs. The time constant for $S_2^{\text{fast}} \rightarrow S_2^{\text{slow}}$ (40 fs) describes the rate with which the fast $S_2 \rightarrow S_1$ channel is quenched. The error estimates given in Figure 2 were obtained from bootstrap resampling of the ensemble populations and fitting the kinetic model to each resample [53].

The employed kinetic model also can be benefi-

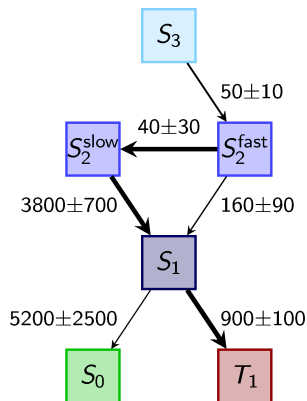


Figure 2: Assumed kinetic model of thymine relaxation, fitted time constants, error estimates and resulting extent of population transfer (indicated by arrow thickness).

cially used to fit the data from our previous simulations of uracil [47] (see the SI for the data and fit). Compared to thymine, in uracil most time constants are slightly faster, with ground state relaxation being much faster at $\tau = 1500$ fs. This difference is most likely due to the missing methyl group of uracil.

Focusing on the results for the singlet multiplicity first, we find that the kinetic model and the fitted time constants agree well with the time constants found in gas phase time-resolved photoelectron experiments, which usually report a fast component around 100 fs and another component of 5-7 ps [19–21, 24, 25, 54]. Here, the fast component could be explained with the fast $S_2(\pi\pi^*) \rightarrow S_1(n\pi^*)$ channel, while the slow component is due to $S_2(\pi\pi^*) \rightarrow S_1(n\pi^*) \rightarrow S_0$ which involves two steps. Our simulations agree with other dynamics studies based on CASSCF calculations [30, 32, 35, 42] in the sense that the experimental few-ps time constant is explained by trapping in $S_1(n\pi^*)$ and $S_2(\pi\pi^*)$. Different from the other studies, our simulations also predict a fast $S_2(\pi\pi^*) \rightarrow S_1(n\pi^*)$ relaxation channel, employed by approximately 20% of the population.

However, it is well known that the CASSCF PES of thymine are qualitatively different from the PES obtained with other levels of theory (e.g., CASPT2 [28, 34, 35, 37, 40, 41, 55], CC2 [28], DFT [56], or OM2/MRCI [39]) Hence, it is questionable whether the observed slow decay from the $S_2(\pi\pi^*)$ state to the $S_1(n\pi^*)$ state and the sequentiality of $S_2(\pi\pi^*) \rightarrow S_1(n\pi^*) \rightarrow S_0$ are correct. Recent MS-CASPT2 studies [28, 34, 35, 37, 40, 41, 55] indicate

that a more accurate model for the relaxation of thymine within the singlet manifold involves a portion of the population decaying directly from $S_2(\pi\pi^*)$ to S_0 (via a CI involving a twist of the C₅-C₆ bond), while another portion crosses to the $^1n\pi^*$ state and gets trapped. The finding that there is no trapping in the $^1\pi\pi^*$ state has also been shown experimentally [26, 27, 57]. The $S_1(n\pi^*)$ population then decays on slower timescales to S_0 , most probably via a recrossing to $S_2(\pi\pi^*)$ and relaxation along the same path as the fast decaying portion [35, 37, 41]. The same model was also proposed for uracil [58].

There exist some studies where the population trapped in the $S_1(n\pi^*)$ minimum has been suggested to be the precursor for ISC [27, 59]. MS-CASPT2 calculations [34] have shown that in the vicinity of the $S_1(n\pi^*)$ minimum two triplet states are energetically close. In this region, the T_1 state has $^3\pi\pi^*$ character while the T_2 state has $^3n\pi^*$ character and thus the T_2 PES is almost parallel to the $S_1(n\pi^*)$ one (see also Figure 3). Close to this region, the characters of the T_2 and T_1 interconvert due to a $T_2/T_1(^3n\pi^*/^3\pi\pi^*)$ crossing. In the vicinity of this coupling region, also a crossing between T_2 (here $^3\pi\pi^*$) and $S_1(n\pi^*)$ is located. These two crossings are hence close to the $S_1(^1n\pi^*)$ minimum and also to the $^3n\pi^*$ minimum. The SOC between $S_1(^1n\pi^*)$ and $T_2(^3\pi\pi^*)$ is reported to be of considerable size (61 cm^{-1}) [34]. This situation is well reproduced at our CASSCF level of theory, since usually states of $n\pi^*$ character are less affected by the missing dynamical electronic correlation in this method and the $^3\pi\pi^*$ state is fortuitously well-described in the surrounding of the $^1,^3n\pi^*$ minima. The SOC in our simulations are also close to the ones reported in the literature [34], peaking at 58 cm^{-1} with an average of 34 cm^{-1} .

Figure 3 shows a linear interpolation in internal coordinates (LIIC) scan from the $S_1(^1n\pi^*)$ minimum to the $S_1/T_2(^1n\pi^*/^3\pi\pi^*)$ minimum energy crossing point on the CASSCF(12,9)/6-31G* level of theory used for the dynamics (starting and end point of the interpolation scan are reported in the SI). Additionally, a LIIC scan carried out at the MS-CASPT2(12,9)/6-31G* level of theory (using MOLCAS 8.0 [60] with an IPEA shift of zero, an imaginary level shift of 0.3 a.u., and the same number of states as in the CASSCF calculations) is shown for comparison. The figure shows that indeed the PES at CASSCF and CASPT2 level agree qualitatively with each other. Hence, we are confi-

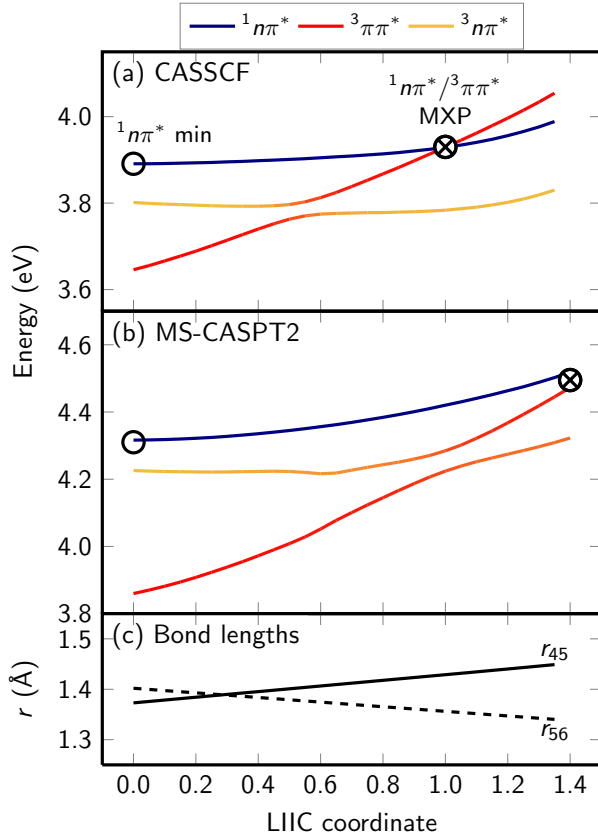


Figure 3: LIIC scan from the S_1 ($^1n\pi^*$) minimum (empty circle) to the S_1/T_2 ($^1n\pi^*/^3\pi\pi^*$) minimum energy crossing point (MXP; circle with cross) and linear extrapolation beyond this point. In (a), the energies of $^1n\pi^*$, $^3n\pi^*$ and $^3\pi\pi^*$ along this scan on the dynamics level of theory (CASSCF(12,9)/6-31G*) are shown, in (b) the same states at the MS-CASPT2(12,9)/6-31G* level of theory (at the same geometries). In (c), the corresponding bond lengths of the $C_4 - C_5$ and $C_5 - C_6$ bonds are plotted.

dent that CASSCF can describe ISC from the $^1n\pi^*$ minimum in a qualitatively correct way.

The S_1/T_2 ($^1n\pi^*/^3\pi\pi^*$) crossing shown in Figure 3 is responsible for the majority of ISC events in the dynamics simulations. We firstly discuss these surface hops in terms of state characters and later on in the frame of MCH states. Out of 53 trajectories showing ISC, 46 trajectories (87%) showed a transition of $^1n\pi^* \rightarrow ^3\pi\pi^*$ type. The remaining trajectories showed $^1n\pi^* \rightarrow ^3n\pi^*$ transitions (4 times) and ISC from the $^1\pi\pi^*$ state (3 times). Hence, the results agree with the expectations from the El-Sayed rule [61]. The small number of $^1n\pi^* \rightarrow ^3n\pi^*$ transitions could be due to the small but non-negligible SOC between these states, or due to mixing of $^3n\pi^*$ and $^3\pi\pi^*$, which would

enhance SOC. When analyzing the ISC transitions in terms of MCH states, we found 13 $S_1 \rightarrow T_1$ hops, 37 $S_1 \rightarrow T_2$ hops, and 3 $S_{2,3} \rightarrow T_2$ hops. Thus, in most cases $^1n\pi^* \rightarrow ^3\pi\pi^*$ transitions involve as a first step a crossing of $^3\pi\pi^*$ and $^3n\pi^*$ (so that $^3\pi\pi^*$ temporarily becomes T_2), followed by $^1n\pi^* \rightarrow ^3\pi\pi^*$ ISC, followed by relaxation in the $^3\pi\pi^*$ via a T_2/T_1 hop. The potential energy scans in Figure 3 visualize how the $^3\pi\pi^*$ gets destabilized along the LIIC coordinate and first crosses with $^3n\pi^*$ and then with $^1n\pi^*$. Note that the fast relaxation via the T_2/T_1 crossing also explains why the T_2 population in Figure 1 never exceed 5%.

Thus, in summary it can be said that ISC in thymine occurs close to the $^1n\pi^*$ minimum at a three-state near-degeneracy region, but involves only the $^1n\pi^*$ and $^3\pi\pi^*$ states, whereas the $^3n\pi^*$ state is mostly a spectator. Other ISC pathways proposed by Serrano-Pérez et al. [34], $^1\pi\pi^* \rightarrow ^3n\pi^*$ and $^1\pi\pi^* \rightarrow ^3\pi\pi^*$, should play only a minor role in thymine. For the $^1\pi\pi^* \rightarrow ^3\pi\pi^*$ pathway, the reported SOC [34] are only 8 cm^{-1} and the crossing occurs far away from any potential energy minimum, thus allowing ISC only for a limited amount of time. Consequently, in our simulations we find only a very small number of ISC hops originating from the $^1\pi\pi^*$ (S_2) state, as opposed to the larger number of ISC hops from $^1n\pi^*$ (S_1). However, our simulations also overestimate the lifetime of the $^1\pi\pi^*$ (S_2) state, and on CASPT2 level the $^1\pi\pi^*$ state is predicted to depopulate very quickly. Hence, we suggest that ISC in thymine does not originate from the $^1\pi\pi^*$, but from the $^1n\pi^*$ state. The latter acts as the doorway state for ISC, as suggested by Hare et al [27, 59]. We note here that Kunitski et al. [25] reported gas phase experiments where they found a 3-exponential decay with time constants of $80 \pm 40 \text{ fs}$, $4.8 \pm 2 \text{ ps}$ and $280 \pm 30 \text{ ns}$ for thymine. They concluded that the long lived dark state (lifetime of hundreds of ns) is of triplet character and that the 4.8 ps time constant is related to ISC. This time constant agrees very well with our simulations—if one assumes a pathway via the “slow” S_2 , the triplet state is populated on a few-ps time scale ($3800 + 900 \text{ fs}$). Note that according to calculations of Etinski et al. [33], this time scale is sensitive to vibrational excess energy, with a possible range of 9 to 770 ps for ISC from a vibrationally cold S_1 state.

Interestingly, in our simulations S_1 ($^1n\pi^*$) $\rightarrow T_2$ ($^3\pi\pi^*$) is more than 5 times as fast as S_1 ($^1n\pi^*$) $\rightarrow S_0$, which would lead to an ISC yield of about 0.85,

much larger than the experimentally measured values [15, 16, 18]. There are several possible reasons for this discrepancy: (1) Based on comparison with CASPT2 calculations [37], S_1 ($^1n\pi^*$) \rightarrow S_0 is most probably too slow on CASSCF level. (2) ISC might actually be slower than predicted by CASSCF. The larger energy difference of the S_1 ($^1n\pi^*$) minimum and the S_1/T_2 ($^1n\pi^*/^3\pi\pi^*$) crossing at CASPT2 (Figure 3 (b)) compared to CASSCF (Figure 3 (a)) would agree with this thought. (3) All experimental ISC yields are measured in solution, while our simulations describe the gas phase situation. According to many authors, for thymine [33, 34, 37, 62] and similarly for uracil [58, 63–65] a more polar solvent destabilizes the $^1n\pi^*$ state compared to $^1\pi\pi^*$, which could reduce the amount of population going through the $^1n\pi^*$ as well as decrease its lifetime. Note that for uracil (essentially thymine without the methyl group), ISC is strongly solvent-dependent, and varies from a few percent in water to about 50% in aprotic, less polar solvents [59, 66]. The gas phase can be seen as truly non-polar and an even higher ISC yield could therefore be expected [47, 48]. Unfortunately, experimental ISC yields for the gas phase are not reported in the literature (neither for uracil nor thymine), according to our knowledge.

Finally, we want to briefly describe the geometric changes seen in the dynamics. The transition from $^1\pi\pi^*$ (S_2) to $^1n\pi^*$ (S_1) is mediated by two different types of crossings in our simulations, as shown by the clustering of the hopping geometries in Figure 4a. Note that these are the geometries where the trajectories hopped from S_2 to S_1 , and that these are not optimized minimum-energy crossing points. However, based on each hopping geometry, an optimization was performed (using the standard algorithm of MOLPRO[67]), leading to either of the two geometries marked with “X” in Figure 4. These latter geometries are hence stationary points on the S_1/S_2 intersection seam, whereas the hopping geometries are simply geometries close to the seam. The majority of the $S_2 \rightarrow S_1$ hops (54 out of 77) were induced by a crossing whose geometry shows a relatively short C_4 -O bond length (atom numbering in panel b, optimized energy: 6.60 eV), depicted by the cluster in the lower right corner of Figure 4a; an exemplary geometry is also shown in panel e. Since this crossing is relatively close to the Franck-Condon region (middle of Figure 4a and geometry in c), some trajectories arrive there early in the dynamics (28 trajectories), which is

the reason for the fast $S_2 \rightarrow S_1$ channel shown in figure 2. The remaining trajectories miss the crossing and get trapped in the S_2 minimum with a long C_4 -O bond (upper right corner, geometry in d). Trajectories leave the S_2 minimum slowly (the slow relaxation channel) and eventually decay to the S_1 , employing either the “short C_4 -O” crossing or another S_2/S_1 crossing. The latter crossing shows rather long C_4 -O bonds and small C_5 - C_4 -O angles (upper left corner in the figure, optimized energy: 6.30 eV), as well as out-of-plane motion of O_4 (“oop- O_4 ”), as can be seen in panel f. The “oop- O_4 ” crossing has been previously reported as “ 6S_5 ” by Szymczak et al. [32], whereas the “short C_4 -O” crossing was not reported so far in the literature, to the best of our knowledge. The two optimized geometries are reported in the SI. Note, however, that—as mentioned before—the described crossings were obtained at CASSCF level, and that at MS-CASPT2 the $S_2 \rightarrow S_1$ relaxation process might be different.

After relaxation to the $^1n\pi^*$ (S_1) minimum, a large fraction of the trajectories undergo ISC. This process is mainly controlled by geometric parameters which strongly destabilize the $^3\pi\pi^*$ state, as was shown in Figure 3 for the $C_5 - C_6$ and $C_4 - C_5$ bond lengths. A shortening of the $C_5 - C_6$ bond for example increases the $^3\pi\pi^*$ energy (see Figure 3), which may facilitate reaching the $^1n\pi^*/^3\pi\pi^*$ crossing. However, based on the trajectories it is not possible to single out an isolated mode of the molecule which is responsible for $^1n\pi^* \rightarrow ^3\pi\pi^*$ ISC. The distribution of geometric parameters of all ISC hopping geometries is not significantly different from the distribution of the same parameters over all trajectories moving in S_1 . This suggests that several modes are strongly coupled in bringing about the $^1n\pi^*/^3\pi\pi^*$ crossing and hence ISC.

It was noted for many trajectories that the state hops induce well observable variations to some vibrational modes. The most prominent of these “indicator modes” were the C_4 -O and C_5 - C_6 bond lengths. Figure 5 shows for an exemplary trajectory the time dependence of these two bonds, together with the moving averages (an average is taken over 50 fs before and 50 fs after the respective point in time in order to obtain smooth curves, which show the trend on this 100 fs time scale). The figure also indicates at which times a state-to-state transition in this trajectory occurred. As can be nicely seen, after excitation to the S_2 state the bond length moving averages quickly (within 50 fs) assume the

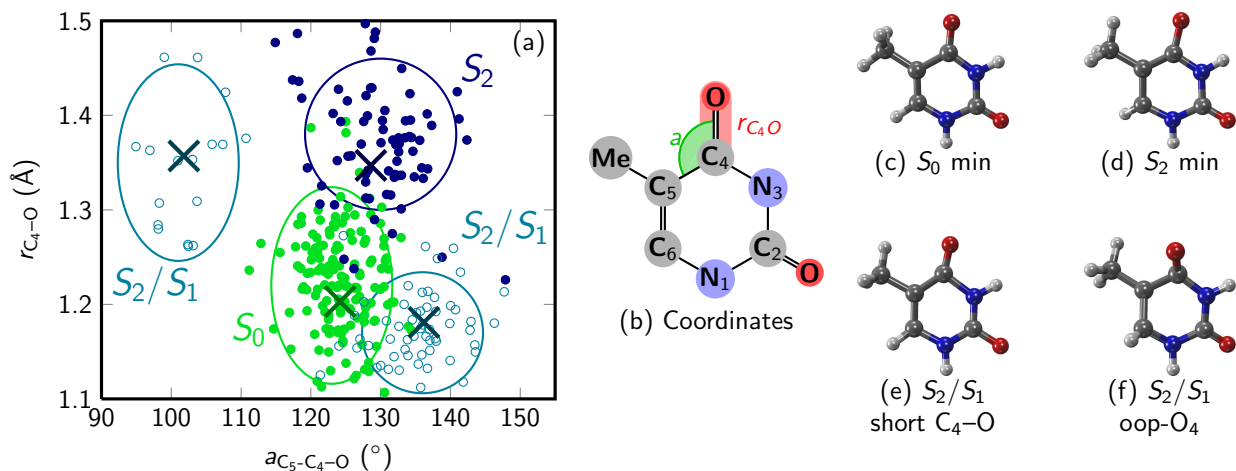


Figure 4: Overview over geometric parameters during internal conversion. In (a) a scatter plot of the C_5-C_4-O angle and C_4-O bond length for initial geometries (S_0 , green), for trajectories trapped in S_2 ($^1\pi\pi^*$, blue), and for S_2/S_1 hopping geometries (open rings). The crosses indicate the location of the corresponding minimum or minimum energy crossing point. In (b), the two internal coordinates are depicted schematically. Panels (c) to (f) show exemplary geometries of S_0 , S_2 , and the two different S_2/S_1 conical intersections.

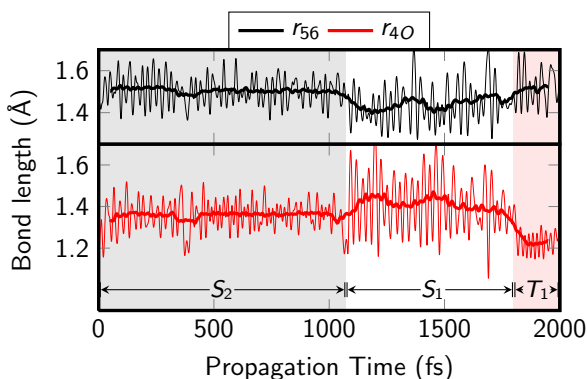


Figure 5: Time dependence of the bond lengths of C_4-O and C_5-C_6 of an exemplary trajectory and moving averages (100 fs width). The shaded areas denote time intervals where the trajectory moved in S_2 , S_1 and T_1 , from left to right.

bond lengths of the S_2 minimum geometry—1.49 Å for r_{56} and 1.35 Å for r_{4O} . At 1080 fs, when the trajectory relaxes to the S_1 state, the average bond lengths change, with r_{56} becoming shorter (the S_1 minimum bond length is 1.42 Å) while r_{4O} increases (minimum at 1.37 Å, the larger average in the figure could be explained by a strong excitation of the bond or anharmonicity). Finally, after ISC to T_1 (minimum values: $r_{56}=1.49$ Å, $r_{4O}=1.22$ Å) again a significant change of the average bond lengths can be seen, especially for the C_4-O bond, which contracted notably.

4. Conclusion

Ab-initio non-adiabatic molecular dynamics simulations including singlet and triplet states using the SHARC methodology have been performed to investigate the intersystem crossing mechanism of thymine. The simulations were based on CASSCF electronic structure calculations. It was found that after initial photoexcitation to the bright $^1\pi\pi^*$ state the majority of trajectories spends considerable time in this state before relaxing to the $^1n\pi^*$. From the latter state, the system relaxes slowly (few ps time scale) to the ground state, which agrees with the findings of previous CASSCF-based dynamics studies [30, 32, 35, 42] and yields excited-state lifetimes in agreement with gas-phase pump-probe spectroscopy [19–21, 24–26, 54]. Additionally, it was simulated for the first time that from

the $^1n\pi^*$ state efficient ISC on a picosecond time scale occurs, bringing the system to the $^3\pi\pi^*$ state. Our simulations also show that other ISC pathways described in the literature [34], $^1\pi\pi^* \rightarrow ^3n\pi^*$ and $^1\pi\pi^* \rightarrow ^3\pi\pi^*$, are not important in the dynamics.

In summary, our results provide evidence that the time-dependent treatment of the relaxation processes in the nucleobase thymine has to include the possibility of ISC in order to fully cover the whole range of important interactions between the different electronic states. However, it is imperative for a more thorough understanding of thymine’s excited-state dynamics that future simulations are based on more accurate electronic structure calculations than CASSCF. Recent dynamics simulations [40, 48, 55] on CASPT2 level of theory are already a step in this direction, but more developments are needed until similar calculations can be carried out routinely.

Acknowledgments

Funding from the Austrian Science Fund (FWF), project P25827, and generous allocation of computer resources at the Vienna Scientific Cluster 2 (VSC2) are gratefully acknowledged. We also thank the COST actions CM1204 (XLIC) and CM1305 (ECOSTBio) for support.

- [1] C. E. Crespo-Hernández, B. Cohen, P. M. Hare, B. Kohler, Ultrafast excited-state dynamics in nucleic acids, *Chem. Rev.* 104 (4) (2004) 1977–2020. doi:10.1021/cr0206770.
- [2] C. T. Middleton, K. de La Harpe, C. Su, Y. K. Law, C. E. Crespo-Hernández, B. Kohler, DNA excited-state dynamics: From single bases to the double helix, *Ann. Rev. Phys. Chem.* 60 (2009) 217–239. doi:10.1146/annurev.physchem.59.032607.093719.
- [3] K. Kleinermanns, D. Nachtigallová, M. S. de Vries, Excited state dynamics of DNA bases, *Int. Rev. Phys. Chem.* 32 (2) (2013) 308–342. doi:10.1080/0144235X.2012.760884.
- [4] M. Barbatti, A. C. Borin, S. Ullrich (Eds.), *Photoinduced Phenomena in Nucleic Acids I*, Vol. 355 of *Topics in Current Chemistry*, Springer Berlin Heidelberg, 2015.
- [5] M. Barbatti, A. C. Borin, S. Ullrich (Eds.), *Photoinduced Phenomena in Nucleic Acids II*, Vol. 356 of *Topics in Current Chemistry*, Springer Berlin Heidelberg, 2015.
- [6] S. Mouret, C. Baudouin, M. Charveron, A. Favier, J. Cadet, T. Douki, Cyclobutane pyrimidine dimers are predominant DNA lesions in whole human skin exposed to UVA radiation, *Proc. Natl. Acad. Sci.* 103 (37) (2006) 13765–13770. doi:10.1073/pnas.0604213103.
- [7] R. Beukers, W. Berends, Isolation and identification of the irradiation product of thymine, *Biochim. Biophys. Acta* 41 (1960) 550–551. doi:10.1016/0006-3002(60)90063-9.
- [8] R. B. Setlow, J. K. Setlow, Evidence that ultraviolet-induced thymine dimers in dna cause biological damage, *Proc. Natl. Acad. Sci. U. S. A.* 48 (1962) 1250–1257. doi:10.1073/pnas.48.7.1250.
- [9] R. B. Setlow, W. L. Carrier, P. A. Swenson, Thymine dimers and inhibition of dna synthesis by ultraviolet irradiation of cells, *Science* 142 (1963) 1464–1466. doi:10.1126/science.142.3598.1464.
- [10] W.-M. Kwok, C. Ma, D. L. Phillips, A doorway state leads to photostability or triplet photodamage in thymine DNA, *J. Am. Chem. Soc.* 130 (15) (2008) 5131–5139. doi:10.1021/ja077831q.
- [11] W. J. Schreier, T. E. Schrader, F. O. Koller, P. Gilch, C. E. Crespo-Hernández, V. N. Swaminathan, T. Charell, W. Zinth, B. Kohler, Thymine dimerization in DNA is an ultrafast photoreaction, *Science* 315 (2007) 625–629. doi:10.1126/science.1135428.
- [12] W. J. Schreier, J. Kubon, N. Regner, K. Haiser, T. E. Schrader, W. Zinth, P. Clivio, P. Gilch, Thymine dimerization in DNA model systems: Cyclobutane photolysis is predominantly formed via the singlet channel, *J. Am. Chem. Soc.* 131 (14) (2009) 5038–5039. doi:10.1021/ja900436t.
- [13] A. Banyasz, T. Douki, R. Improta, T. Gustavsson, D. Onidas, I. Vayá, M. Perron, D. Markovitsi, Electronic excited states responsible for dimer formation upon UV absorption directly by thymine strands: Joint experimental and theoretical study, *J. Am. Chem. Soc.* 134 (36) (2012) 14834–14845. doi:10.1021/ja304069f.
- [14] L. Liu, B. M. Pilles, J. Gontcharov, D. B. Bucher, W. Zinth, Quantum yield of cyclobutane pyrimidine dimer formation via the triplet channel determined by photosensitization, *J. Phys. Chem. B* 120 (2) (2016) 292–298. doi:10.1021/acs.jpcc.5b08568.
- [15] H. E. Johns, D. W. Whillans, Properties of the triplet states of thymine and uracil in aqueous solution, *J. Am. Chem. Soc.* 93 (6) (1971) 1358–1362. doi:10.1021/ja00735a007.
- [16] C. Salet, R. Bensasson, Studies on thymine and uracil triplet excited state in acetonitrile and water, *Photochem. Photobiol.* 22 (6) (1975) 231–235. doi:10.1111/j.1751-1097.1975.tb06741.x.
- [17] K. Röttger, H. Marroux, H. Böhnke, D. Morris, A. Voice, F. Temps, G. M. Roberts, A. Orr-Ewing, Probing the excited state relaxation dynamics of pyrimidine nucleosides in chloroform solution, *Faraday Discuss.* (2016) DOI: 10.1039/C6FD00068A. doi:10.1039/C6FD00068A.
- [18] A. A. Lamola, J. P. Mittal, Solution photochemistry of thymine and uracil, *Science* 154 (3756) (1966) 1560–1561. doi:10.1126/science.154.3756.1560.
- [19] H. Kang, K. T. Lee, B. Jung, Y. J. Ko, S. K. Kim, Intrinsic lifetimes of the excited state of DNA and RNA bases, *J. Am. Chem. Soc.* 124 (44) (2002) 12958–12959. doi:10.1021/ja027627x.
- [20] S. Ullrich, T. Schultz, M. Z. Zgierski, A. Stolow, Electronic relaxation dynamics in DNA and RNA bases studied by time-resolved photoelectron spectroscopy, *Phys. Chem. Chem. Phys.* 6 (10) (2004) 2796–2801. doi:10.1039/B316324E.
- [21] C. Canuel, M. Mons, F. Piuze, B. Tardivel, I. Dimicoli, M. Elhanine, Excited states dynamics of DNA and RNA bases: Characterization of a stepwise deactivation pathway in the gas phase, *J. Chem. Phys.* 122 (7) (2005) 074316. doi:10.1063/1.1850469.

- [22] Y. He, C. Wu, W. Kong, Decay pathways of thymine and methyl-substituted uracil and thymine in the gas phase, *J. Phys. Chem. A* 107 (26) (2003) 5145–5148. doi:10.1021/jp034733s.
- [23] Y. He, C. Wu, W. Kong, Photophysics of methyl-substituted uracils and thymines and their water complexes in the gas phase, *J. Phys. Chem. A* 108 (6) (2004) 943–949. doi:10.1021/jp036553o.
- [24] E. Samoylova, T. Schultz, I. Hertel, W. Radloff, Analysis of ultrafast relaxation in photoexcited DNA base pairs of adenine and thymine, *Chem. Phys.* 347 (1–3) (2008) 376–382. doi:10.1016/j.chemphys.2007.09.046.
- [25] M. Kunitski, Y. Nosenko, B. Brutschy, On the nature of the long-lived "dark" state of isolated 1-methylthymine, *ChemPhysChem* 12 (10) (2011) 2024–2030. doi:10.1002/cphc.201000985.
- [26] B. McFarland, J. Farrell, S. Miyabe, F. Tarantelli, A. Aguilar, N. Berrah, C. Bostedt, J. Bozek, P. Bucksbaum, J. Castagna, R. Coffee, J. Cryan, L. Fang, R. Feifel, K. Gaffney, J. Glowina, T. Martinez, M. Mucke, B. Murphy, A. Natan, T. Osipov, V. Petrović, S. Schorb, T. Schultz, L. Spector, M. Swiggers, I. Tenney, S. Wang, J. White, W. White, M. Gühr, Ultrafast x-ray auger probing of photoexcited molecular dynamics, *Nat. Commun.* 5 (2014) 4235. doi:10.1038/ncomms5235.
- [27] P. M. Hare, C. E. Crespo-Hernández, B. Kohler, Internal conversion to the electronic ground state occurs via two distinct pathways for pyrimidine bases in aqueous solution, *Proc. Natl. Am. Soc.* 104 (2) (2007) 435–440. doi:10.1073/pnas.0608055104.
- [28] S. Perun, A. L. Sobolewski, W. Domcke, Conical intersections in thymine, *J. Phys. Chem. A* 110 (49) (2006) 13238–13244. doi:10.1021/jp0633897.
- [29] G. Zechmann, M. Barbatti, Photophysics and deactivation pathways of thymine, *J. Phys. Chem. A* 112 (36) (2008) 8273–8279. doi:10.1021/jp804309x.
- [30] H. R. Hudock, B. G. Levine, A. L. Thompson, H. Satzger, D. Townsend, N. Gador, S. Ullrich, A. Stolow, T. J. Martínez, Ab initio molecular dynamics and time-resolved photoelectron spectroscopy of electronically excited uracil and thymine, *J. Phys. Chem. A* 111 (34) (2007) 8500–8508. doi:10.1021/jp0723665.
- [31] J. González-Vázquez, L. González, E. Samoylova, T. Schultz, Thymine relaxation after uv irradiation: The role of tautomerization and $\pi\sigma^*$ states, *Phys. Chem. Chem. Phys.* 11 (2009) 3927–3934. doi:10.1039/b815602f.
- [32] J. J. Szymczak, M. Barbatti, J. T. Soo Hoo, J. A. Adkins, T. L. Windus, D. Nachtigallova, H. Lischka, Photodynamics simulations of thymine: Relaxation into the first excited singlet state, *J. Phys. Chem. A* 113 (45) (2009) 12686–12693. doi:10.1021/jp905085x.
- [33] M. Etinski, T. Fleig, C. M. Marian, Intersystem crossing and characterization of dark states in the pyrimidine nucleobases uracil, thymine, and 1-methylthymine, *J. Phys. Chem. A* 113 (43) (2009) 11809–11816. doi:10.1021/jp902944a.
- [34] J. J. Serrano-Pérez, R. González-Luque, M. Merchán, L. Serrano-Andrés, On the intrinsic population of the lowest triplet state of thymine, *J. Phys. Chem. B* 111 (2007) 11880–11883. doi:10.1021/jp0765446.
- [35] D. Asturiol, B. Lasorne, M. A. Robb, L. Blancafort, Photophysics of the π, π^* and n, π^* states of thymine: MS-CASPT2 minimum-energy paths and CASSCF on-the-fly dynamics, *J. Phys. Chem. A* 113 (38) (2009) 10211–10218. doi:10.1021/jp905303g.
- [36] M. Merchán, R. González-Luque, T. Climent, L. Serrano-Andrés, E. Rodríguez, M. Reguero, D. Peláez, Unified model for the ultrafast decay of pyrimidine nucleobases, *J. Phys. Chem. B* 110 (51) (2006) 26471–26476. doi:10.1021/jp066874a.
- [37] S. Yamazaki, T. Taketsugu, Nonradiative deactivation mechanisms of uracil, thymine, and 5-fluorouracil: A comparative ab initio study, *J. Phys. Chem. A* 116 (1) (2012) 491–503. doi:10.1021/jp206546g.
- [38] R. González-Luque, T. Climent, I. González-Ramírez, M. Merchán, L. Serrano-Andrés, Singlet and Triplet states interaction regions in DNA/RNA nucleobase hypersurfaces, *J. Chem. Theory Comput.* 6 (7) (2010) 2103–2114. doi:10.1021/ct100164m.
- [39] Z. Lan, E. Fabiano, W. Thiel, Photoinduced nonadiabatic dynamics of pyrimidine nucleobases: On-the-fly surface-hopping study with semiempirical methods, *J. Phys. Chem. B* 113 (11) (2009) 3548–3555. doi:10.1021/jp809085h.
- [40] A. Nakayama, G. Arai, S. Yamazaki, T. Taketsugu, Solvent effects on the ultrafast nonradiative deactivation mechanisms of thymine in aqueous solution: Excited-state QM/MM molecular dynamics simulations, *J. Chem. Phys.* 139 (21) (2013) 214304. doi:10.1063/1.4833563.
- [41] D. Asturiol, B. Lasorne, G. A. Worth, M. A. Robb, L. Blancafort, Exploring the sloped-to-peaked S_2/S_1 seam of intersection of thymine with electronic structure and direct quantum dynamics calculations, *Phys. Chem. Chem. Phys.* 12 (2010) 4949–4958. doi:10.1039/C001556C.
- [42] M. Barbatti, A. J. A. Aquino, J. J. Szymczak, D. Nachtigallova, P. Hobza, H. Lischka, Relaxation mechanisms of UV-Photoexcited DNA and RNA nucleobases, *P. Natl. Acad. Sci. USA* 107 (50) (2010) 21453–21458. doi:10.1073/pnas.1014982107.
- [43] M. Richter, P. Marquetand, J. González-Vázquez, I. Sola, L. González, SHARC: Ab initio molecular dynamics with surface hopping in the adiabatic representation including arbitrary couplings, *J. Chem. Theory Comput.* 7 (5) (2011) 1253–1258. doi:10.1021/ct1007394.
- [44] S. Mai, P. Marquetand, L. González, A general method to describe intersystem crossing dynamics in trajectory surface hopping, *Int. J. Quantum Chem.* 115 (18) (2015) 1215–1231. doi:10.1002/qua.24891.
- [45] S. Mai, M. Richter, M. Ruckebauer, M. Oppel, P. Marquetand, L. González, SHARC: Surface hopping including arbitrary couplings – program package for non-adiabatic dynamics, *sharc-md.org* (2014).
- [46] S. Mai, P. Marquetand, M. Richter, J. González-Vázquez, L. González, Singlet and triplet excited-state dynamics study of the keto and enol tautomers of cytosine, *ChemPhysChem* 14 (2013) 2920–2931. doi:10.1002/cphc.201300370.
- [47] M. Richter, S. Mai, P. Marquetand, L. González, Ultrafast intersystem crossing dynamics in uracil unravelled by ab initio molecular dynamics, *Phys. Chem. Chem. Phys.* 16 (2014) 24423–24436. doi:10.1039/C4CP04158E.
- [48] S. Mai, P. Marquetand, L. González, Intersystem crossing pathways in the noncanonical nu-

- cleobase 2-thiouracil: A time-dependent picture, *J. Phys. Chem. Lett.* 7 (0) (2016) 1978–1983. doi:10.1021/acs.jpcllett.6b00616.
- [49] J. C. Tully, Molecular dynamics with electronic transitions, *J. Chem. Phys.* 93 (2) (1990) 1061–1071. doi:10.1063/1.459170.
- [50] H.-J. Werner, P. J. Knowles, G. Knizia, F. R. Manby, M. Schütz, P. Celani, T. Korona, R. Lindh, A. Mitrushenkov, G. Rauhut, K. R. Shamasundar, T. B. Adler, R. D. A. A. Bernhardtsson, A. Berning, D. L. Cooper, M. J. O. Deegan, A. J. Dobson, F. Eckert, E. Goll, C. Hampel, A. Hesselmann, G. Hetzer, T. Hrenar, G. Jansen, C. Köppland, Y. Liu, A. W. Lloyd, R. A. Mata, A. J. May, S. J. McNicholas, W. Meyer, M. E. Mura, A. Nicklass, D. P. O’Neill, P. Palmieri, D. Peng, K. Pflüger, R. Pitzerand, M. Reiher, T. Shiozaki, H. Stoll, A. J. Stone, R. Tarroni, T. Thorsteinsson, M. Wang, Molpro, version 2012.1, a package of ab initio programs, see <https://www.molpro.net/> (2012).
- [51] B. P. Fingerhut, K. E. Dorfman, S. Mukamel, Probing the conical intersection dynamics of the rna base uracil by uv-pump stimulated-raman-probe signals; ab initio simulations, *J. Chem. Theory Comput.* 10 (2014) 1172–1188. doi:10.1021/ct401012u.
- [52] Barbatti, M., Granucci, G., Persico, M., Ruckebauer, M., Vazdar, M., Eckert-Maksic, M., Lischka, H., The on-the-fly surface-hopping program system Newton-X: Application to ab initio simulation of the nonadiabatic photodynamics of benchmark systems, *J. Photochem. Photobiol. A* 190 (2007) 228–240. doi:10.1016/j.jphotochem.2006.12.008.
- [53] S. Nangia, A. W. Jasper, T. F. Miller, D. G. Truhlar, Army ants algorithm for rare event sampling of delocalized nonadiabatic transitions by trajectory surface hopping and the estimation of sampling errors by the bootstrap method, *J. Chem. Phys.* 120 (8) (2004) 3586–3597. doi:10.1063/1.1641019.
- [54] H. Yu, J. A. Sánchez-Rodríguez, M. Pollum, C. E. Crespo-Hernández, S. Mai, P. Marquetand, L. González, S. Ullrich, Internal conversion and intersystem crossing pathways in UV excited, isolated uracils and their implications in prebiotic chemistry, *Phys. Chem. Chem. Phys.* 18 (2016) 20168–20176. doi:10.1039/C6CP01790H.
- [55] F. Buchner, A. Nakayama, S. Yamazaki, H.-H. Ritze, A. Lübcke, Excited-state relaxation of hydrated thymine and thymidine measured by liquid-jet photoelectron spectroscopy: Experiment and simulation, *J. Am. Chem. Soc.* 137 (8) (2015) 2931–2938. doi:10.1021/ja511108u.
- [56] D. Picconi, V. Barone, A. Lami, F. Santoro, R. Improta, The interplay between $\pi\pi^*/n\pi^*$ excited states in gas-phase thymine: A quantum dynamical study, *ChemPhysChem* 12 (2011) 1957–1968. doi:10.1002/cphc.201001080.
- [57] O. Gessner, M. Gühr, Monitoring ultrafast chemical dynamics by time-domain X-ray photo- and auger-electron spectroscopy, *Acc. Chem. Res.* 49 (1) (2016) 138–145. doi:10.1021/acs.accounts.5b00361.
- [58] Y. Mercier, F. Santoro, M. Reguero, R. Improta, The decay from the dark $n\pi^*$ excited state in uracil: An integrated caspt2/casscf and pcm/td-dft study in the gas phase and in water, *J. Phys. Chem. B* 112 (2008) 10769–10772.
- [59] P. M. Hare, C. E. Crespo-Hernández, B. Kohler, Solvent-dependent photophysics of 1-cyclohexyluracil: Ultrafast branching in the initial bright state leads non-radiatively to the electronic ground state and a long-lived $1n\pi^*$ state, *J. Phys. Chem. B* 110 (37) (2006) 18641–18650. doi:10.1021/jp064714t.
- [60] F. Aquilante, J. Autschbach, R. K. Carlson, L. F. Chibotaru, M. G. Delcey, L. De Vico, I. Fdez. Galván, N. Ferré, L. M. Frutos, L. Gagliardi, M. Garavelli, A. Giussani, C. E. Hoyer, G. Li Manni, H. Lischka, D. Ma, P.-Å. Malmqvist, T. Müller, A. Nenov, M. Olivucci, T. B. Pedersen, D. Peng, F. Plasser, B. Pritchard, M. Reiher, I. Rivalta, I. Schapiro, J. Segarra-Martí, M. Stenrup, D. G. Truhlar, L. Ungur, A. Valentini, S. Vancocille, V. Veryazov, V. P. Vysotskiy, O. Weingart, F. Zapata, R. Lindh, Molcas 8: New capabilities for multiconfigurational quantum chemical calculations across the periodic table, *J. Comput. Chem.* 37 (2015) 506–541. doi:10.1002/jcc.24221.
- [61] M. A. El-Sayed, Spin-orbit coupling and the radiationless processes in nitrogen heterocyclics, *J. Chem. Phys.* 38 (12) (1963) 2834–2838. doi:10.1063/1.1733610.
- [62] T. Gustavsson, A. Bányász, E. Lazzarotto, D. Markovitsi, G. Scalmani, M. J. Frisch, V. Barone, R. Improta, Singlet excited-state behavior of uracil and thymine in aqueous solution: A combined experimental and computational study of 11 uracil derivatives, *J. Am. Chem. Soc.* 128 (2) (2006) 607–619. doi:10.1021/ja056181s.
- [63] K. A. Kistler, S. Matsika, Solvatochromic shifts of uracil and cytosine using a combined multireference configuration interaction/molecular dynamics approach and the fragment molecular orbital method, *J. Phys. Chem. A* 113 (45) (2009) 12396–12403. doi:10.1021/jp901601u.
- [64] J. M. Olsen, K. Aidas, K. V. Mikkelsen, J. Kongsted, Solvatochromic shifts in uracil: A combined MD-QM/MM study, *J. Chem. Theory Comput.* 6 (1) (2010) 249–256. doi:10.1021/ct900502s.
- [65] A. DeFusco, J. Ivanic, M. W. Schmidt, M. S. Gordon, Solvent-induced shifts in electronic spectra of uracil, *J. Phys. Chem. A* 115 (18) (2011) 4574–4582. doi:10.1021/jp112230f.
- [66] M. M. Brister, C. E. Crespo-Hernández, Direct observation of triplet-state population dynamics in the RNA uracil derivative 1-cyclohexyluracil, *J. Phys. Chem. Lett.* 6 (21) (2015) 4404–4409. doi:10.1021/acs.jpcllett.5b01901.
- [67] M. J. Bearpark, M. A. Robb, H. B. Schlegel, A direct method for the location of the lowest energy point on a potential surface crossing, *Chem. Phys. Lett.* 223 (1994) 269. doi:10.1016/0009-2614(94)00433-1.

Supporting Information for: The DNA Nucleobase Thymine in Motion – Intersystem Crossing Simulated with Surface Hopping

Sebastian Mai^a, Martin Richter^{a,1}, Philipp Marquetand^{a,*}, Leticia González^{a,*}

^a Institute of Theoretical Chemistry, Faculty of Chemistry, University of Vienna, Währinger Str. 17, 1090 Vienna, Austria.

¹ Present address: Max-Born-Institute for Nonlinear Optics and Ultrafast Pulse Spectroscopy, 12489 Berlin, Germany.

* Corresponding author

Email addresses: philipp.marquetand@univie.ac.at (Philipp Marquetand), leticia.gonzalez@univie.ac.at (Leticia González)

1. Level of Theory Validation

Table S1 presents the energies and energy gaps for several critical points on thymine’s potential energy surfaces (PESs). In the “CASSCF” column, the same level of theory as in the dynamics simulations is used. In the right-most columns, MS-CASPT2 results are presented for comparison. The latter computations employed MOLCAS 8.0, a CAS(12,9), the 6-31G* basis set, 4 singlet or 3 triplet states in the state-averaging (SA over singlets and triplets in one calculation is not possible in MOLCAS), an IPEA shift of zero, and an imaginary level shift of 0.3 a.u. The same MS-CASPT2 settings were also used for the LIIC scan presented in the main manuscript. Note that both sets of calculations employed the same geometries, no reoptimization at MS-CASPT2 level was performed.

As can be seen, at the Franck-Condon geometry, CASSCF predicts all vertical excitation energies reasonably well, with the exception of the S_2 ($^1\pi\pi^*$) state, which is predicted 2 eV too high. Also for the minimum geometries, the S_1 ($^1n\pi^*$) and T_1 ($^3\pi\pi^*$) states are well reproduced, whereas the S_2 ($^1\pi\pi^*$) minimum is significantly too high in energy. Furthermore, at CASPT2 level the $^1\pi\pi^*$ minimum has been located on the S_1 surface.[S1]

The crossing points in the singlet manifold do not agree well with each other. However, as the MS-CASPT2 results do not show crossings at these particular geometries, only a proper optimization of the MECPs at MS-CASPT2 level would allow for a full comparison. Still, the results clearly indicate that some details of the $S_2 \rightarrow S_1 \rightarrow S_0$ relaxation of thymine might not be well reproduced by our calculations.

Interestingly, the S_1/T_2 MECP is reasonably described by CASSCF, as can also be seen in Figure 3 in the main manuscript. This fact, together with the qualitatively correct description of the S_1 ($^1n\pi^*$) minimum, indicates that intersystem crossing should be well described in our simulations.

Table S1: Energies of critical points at CASSCF and MS-CASPT2 levels of theory. Energies are given in eV, relative to the S_0 minimum energy (given in Hartree). Energy gaps are given in eV. For crossings, the average energy of the two involved states is given.

Geometry	SA-CASSCF(12,9)/6-31G*		MS-CASPT2(12,9)/6-31G*	
	Energy	Gap	Energy	Gap
S_0 at S_0 min	-451.7938159	—	-452.8009802	—
S_1 ($^1n\pi^*$) at S_0 min	5.14	—	5.10	—
S_2 ($^1\pi\pi^*$) at S_0 min	7.20	—	5.19	—
T_1 ($^3\pi\pi^*$) at S_0 min	3.99	—	3.93	—
T_2 ($^3n\pi^*$) at S_0 min	4.95	—	4.96	—
S_1 ($^1n\pi^*$) min	3.89	—	4.18	—
S_2 ($^1\pi\pi^*$) min	5.85	—	4.86	—
T_1 ($^3\pi\pi^*$) min	3.09	—	3.21	—
S_2/S_1 MECP (oop- O_4)	6.30	<0.01	6.50	0.24
S_2/S_1 MECP (short C_4-O)	6.60	0.01	5.47	0.75
S_1/S_0 MECP (boat)	5.32	0.03	5.14	0.62
S_1/S_0 MECP (oop- O_4)	5.46	<0.01	5.31	0.34
S_1/T_2 MECP	3.93	<0.01	4.25	0.13

2. Details on the Kinetic Model Fitting

The kinetic model used for the population fit is described by the following differential equation system:

$$\frac{\partial}{\partial t} \begin{pmatrix} S_3(t) \\ S_2^{\text{fast}}(t) \\ S_2^{\text{slow}}(t) \\ S_1(t) \\ S_0(t) \\ T_1(t) \end{pmatrix} = \begin{pmatrix} -k_{S_3} & & & & & \\ +k_{S_3} & -(k_{\text{cool}} + k_{\text{d.fast}}) & & & & \\ & +k_{\text{cool}} & -k_{\text{d.slow}} & & & \\ & +k_{\text{d.fast}} & +k_{\text{d.slow}} & -(k_{\text{Rlx}} + k_{\text{ISC}}) & & \\ & & & +k_{\text{Rlx}} & 0 & \\ & & & +k_{\text{ISC}} & & 0 \end{pmatrix} \cdot \begin{pmatrix} S_3(t) \\ S_2^{\text{fast}}(t) \\ S_2^{\text{slow}}(t) \\ S_1(t) \\ S_0(t) \\ T_1(t) \end{pmatrix}, \quad (1)$$

where $S_3(t)$, $S_2^{\text{fast}}(t)$, $S_2^{\text{slow}}(t)$, $S_1(t)$, $S_0(t)$, and $T_1(t)$ are the *model functions* of the respective kinetic species at time t . The k 's are the kinetic constants, where k_{S_3} is the decay constant of $S_3(t)$, k_{cool} the conversion rate for $S_2^{\text{fast}} \rightarrow S_2^{\text{slow}}$, $k_{\text{d.fast}}$ is the decay constant of S_2^{fast} to S_1 , $k_{\text{d.slow}}$ is the decay constant of S_2^{slow} to S_1 , k_{Rlx} is the $S_1 \rightarrow S_0$ constant, and k_{ISC} is the $S_1 \rightarrow T_1$ constant.

The differential equation system has been solved using the computer algebra system MAXIMA 5.29.1, yielding the analytical expressions of the six model functions $S_3(t)$, $S_2^{\text{fast}}(t)$, $S_2^{\text{slow}}(t)$, $S_1(t)$, $S_0(t)$, and $T_1(t)$. The initial values are:

$$\begin{aligned} S_3(0) &= 47/150 \\ S_2^{\text{fast}}(0) &= 103/150 \\ S_2^{\text{slow}}(0) &= 0 \\ S_1(t) &= 0 \\ S_0(t) &= 0 \\ T_1(t) &= 0, \end{aligned}$$

in accordance with the initial distribution of the trajectories.

In a global fitting procedure, using GNUPLOT with the Marquardt-Levenberg algorithm, the actual populations from the simulations were fitted to the model functions, as given below:

$$\begin{aligned} S_3(t) &\Rightarrow S_3^{\text{simulated}}(t) \\ S_2^{\text{fast}} + S_2^{\text{slow}} &\Rightarrow S_2^{\text{simulated}}(t) \\ S_1(t) &\Rightarrow S_1^{\text{simulated}}(t) \\ S_0(t) &\Rightarrow S_0^{\text{simulated}}(t) \\ T_1(t) &\Rightarrow T_1^{\text{simulated}}(t), \end{aligned}$$

where $A \Rightarrow A^{\text{simulated}}$ indicates a least-squares fit, where the constants k_i are varied to minimize $\sum_i (A(t_i) - A^{\text{simulated}}(t_i))^2$.

Here, we want to note that according to this procedure, we do not divide the S_2 population in the trajectory simulations into subpopulations. S_2^{fast} and S_2^{slow} are simply two functions used to model the biexponential decay behaviour of the S_2 population. The actual reason for this behaviour could be that part of the S_2 population in our simulations directly moves from the Franch-Condon point to the S_2/S_1 crossing, whereas the remaining part of the population moves to the S_2 minimum and spends more time until it hits the crossing.

Fitting of the Populations of Uracil

As mentioned in the main manuscript, the biexponential kinetic model can also be utilized for fitting the excited-state populations of uracil, from our previous publication [S2]. Since we did not report such a fit in that paper, we present the fit here, in order to facilitate comparison with the new thymine results.

The populations and time constants are shown in Figure S1. For comparison, in our previous publication [S2] two time constants of 63 fs and 2.8 ps were reported, based on a biexponential fit of the sum of the $S_{\geq 1}$ and $T_{\geq 2}$ states.

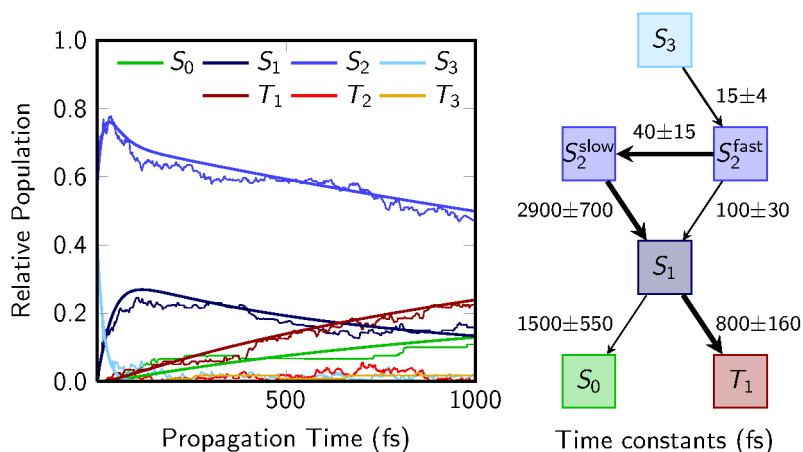


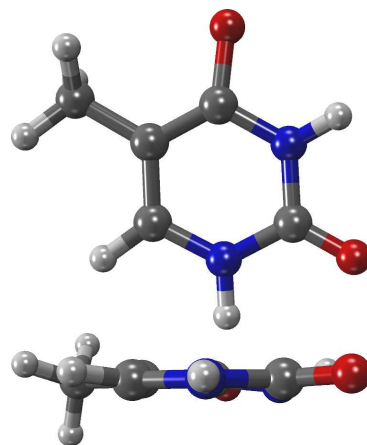
Figure S1: Excited-state populations of uracil (reproduced from Ref. [S2], ensemble II with 120 trajectories and CASSCF(14,10)/6-31G*) and fitted time constants with the kinetic model used here for thymine.

3. Molecular Geometries

15

S1(1npi*) min, SA(4,3)-CASSCF(12,9)/6-31G*

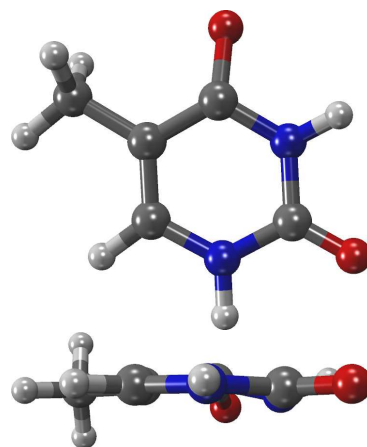
C +0.205075 -0.712113 +0.070989
 C -1.063288 -0.207545 +0.190055
 C -0.337862 +2.103204 +0.060884
 C +1.239085 +0.226715 -0.075745
 C +0.474159 -2.197674 +0.049309
 N -1.342937 +1.156555 +0.082576
 N +0.923657 +1.592693 -0.059017
 O -2.196475 -0.971207 +0.201165
 O -0.569397 +3.279246 +0.133363
 H -2.223892 +1.497048 +0.398503
 H +1.645748 +2.273282 -0.113300
 H +2.277709 -0.023075 -0.048640
 H -0.103455 -2.716011 +0.805912
 H +1.521704 -2.395086 +0.243032
 H +0.225882 -2.629489 -0.914504



15

S1(1npi*)/T2(3pypi*) MXP, SA(4,3)-CASSCF(12,9)/6-31G*

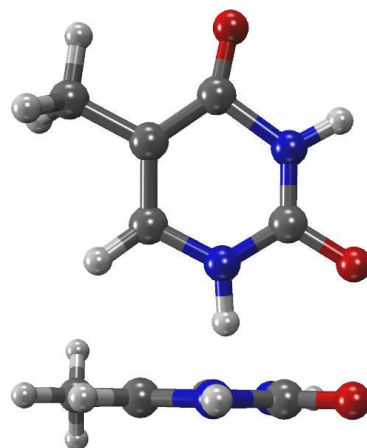
C +0.233164 -0.706194 +0.061724
 C -1.086403 -0.206851 +0.269150
 C -0.339679 +2.098509 +0.031765
 C +1.221543 +0.220027 -0.041484
 C +0.481985 -2.192006 +0.012373
 N -1.348890 +1.153427 +0.030530
 N +0.926517 +1.588056 -0.029929
 O -2.173128 -0.970180 -0.094949
 O -0.571619 +3.275639 +0.077642
 H -2.218321 +1.521499 +0.351851
 H +1.655075 +2.262179 -0.069968
 H +2.259004 -0.030520 -0.124679
 H +0.144294 -2.680543 +0.920435
 H +1.540309 -2.404191 -0.105586
 H -0.042643 -2.639868 -0.822794



15

S1(1npi*)/S2(1pipi*) MXP (short C4-0), SA(4,3)-CASSCF(12,9)/6-31G*

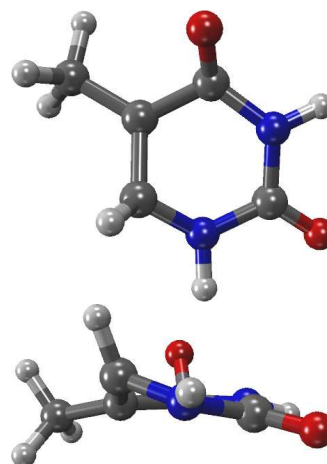
C +0.106693 +0.688813 +0.038900
C -1.232698 +0.306944 +0.203065
C -0.340262 -2.032130 -0.033894
C +1.212306 -0.207715 -0.013595
C +0.405275 +2.163353 -0.007630
N -1.337394 -1.230552 +0.171881
N +0.893983 -1.590127 -0.186102
O -2.268944 +0.856316 +0.344463
O -0.529580 -3.348524 -0.103759
H -2.256217 -1.607073 +0.293248
H +1.612443 -2.266239 -0.330276
H +2.127125 +0.067920 -0.504366
H +0.804265 +2.462921 -0.980805
H -0.502267 +2.728739 +0.173192
H +1.143055 +2.446230 +0.746062



15

S1(1npi*)/S2(1pipi*) MXP (oop-04), SA(4,3)-CASSCF(12,9)/6-31G*

C +0.011564 +0.742077 +0.085354
C -1.309650 +0.161045 +0.048796
C -0.311824 -2.080382 +0.209688
C +1.088845 -0.162168 -0.404492
C +0.273546 +2.186433 +0.364423
N -1.390626 -1.239524 +0.076847
N +0.917867 -1.485542 +0.008556
O -1.944105 +0.821799 -0.936271
O -0.426346 -3.249633 +0.455370
H -2.268376 -1.664645 +0.277842
H +1.651361 -2.141337 -0.146732
H +1.496444 -0.016334 -1.396533
H +1.064885 +2.272661 +1.104756
H +0.606804 +2.714567 -0.525221
H -0.613520 +2.678864 +0.740597



[S1] Yamazaki, S.; Taketsugu, T. *J. Phys. Chem. A* **2012**, *116*, 491–503

[S2] Richter, M.; Mai, S.; Marquetand, P.; González, L. *Phys. Chem. Chem. Phys.* **2014**, *16*, 24423–24436